Modeling Wheat Rust Spread Using Physics-informed Neural Networks for Improved Agricultural Management

Hangjing Xiong[1], Xia Li[1], Di Yuan[1], Jianglong Shen[1, 2, *]
[1]School of Mathematics and Physics, Yibin University, Yibin 644000, China
[2]Key Laboratory of Degraded and Unused Land Consolidation Engineering, Ministry of Natural Resources, Xi'an 710075, China
*Corresponding email: 2024090003@yibinu.edu.cn

Abstract

Wheat rust, a major threat to global agricultural production, necessitates accurate modeling of its spatiotemporal dynamics for effective disease management. This study proposes a novel Physics-Informed Neural Network (PINN) model to predict wheat rust spread, achieving enhanced accuracy through innovative model design and network construction. The model incorporates a dynamic weighted loss function and stratified sampling strategy, effectively balancing initial conditions and physical constraints while improving modeling accuracy near infection foci and domain boundaries. Additionally, a seasonal environmental factor is introduced to enhance biological realism. In network construction, a deep five-layer PINN architecture is employed, optimized with boundary condition-enhanced training and L2 regularization to accurately capture nonlinear dynamics. Experimental results demonstrate high consistency with numerical solutions over a 200-day simulation period, with a mean absolute error below 0.013500 and PDE residuals tightly distributed around zero, validating the model's physical consistency. This study provides a high-precision predictive tool for the spatiotemporal spread of wheat rust, offering scientific guidance for disease control strategies and opening new avenues for agricultural disease modeling.

Keywords

Wheat rust, Physics-Informed Neural Network, Stratified sampling strategy, L2 regularization

Introduction

Wheat rust, a significant fungal disease, poses a severe threat to wheat crops, markedly impacting global wheat production. It spreads rapidly during the wheat growing season, causing serious damage to wheat leaves, stems and ears. This disease can significantly reduce the yield and quality of wheat, posing a serious threat to agricultural production. The transmission routes of wheat rust mainly include wind transmission and direct contact transmission between host plants. Wind transmission is its main mode of transmission. The summer spores of the pathogen can be transmitted through the air, up to hundreds of kilometers away, especially in warm and humid climates, and the transmission speed is more rapid. In addition, the disease can also be transmitted through direct contact between infected wheat plants and healthy plants. The infection of this disease usually occurs at various stages of wheat growth, especially in winter and spring. When environmental conditions are suitable, the spread of rust is rapid, seriously affecting the growth and development of crops. This rapidly spreading pathogen can lead to substantial yield losses, particularly in regions with favorable climatic conditions [1-3]. Research indicates that wheat rust ranks among the top five crop diseases worldwide, with potential yield reductions reaching up to 62%, presenting a formidable challenge to agricultural economies globally [4]. Traditionally, disease spread has been forecasted using field surveys and statistical models. However, these approaches are often hampered by limited data availability and the intricacies of spatial-dynamic modeling. While much of the existing literature has long concentrated on the etiology and chemical management of wheat rust, studies addressing refined space-time dynamic modeling remain scarce [5-7].

Numerical techniques, such as the finite difference method, have been employed to solve reaction-diffusion

equations governing disease spread. Yet, these methods struggle to adapt to complex boundary conditions and scenarios with sparse data. Similarly, machine learning approaches like convolutional neural networks (CNNs) have shown promise in disease detection but often lack the integration of physical laws, making it challenging to capture the underlying mechanisms of disease transmission [8]. In recent years, Physics-Informed Neural Networks (PINNs) have emerged as a powerful tool, offering a novel framework for tackling complex dynamic systems in agricultural ecosystems [9,10]. By embedding physical laws as regularization terms, PINNs enhance model generalization, particularly in data-scarce environments. Although PINNs have gained traction in fields like engineering and physics, their application in plant pathology and ecological modeling remains largely unexplored, opening up exciting opportunities for innovative research [11,12].

This study leverages PINNs to model the spatiotemporal dynamics of wheat rust dissemination on a global scale, effectively integrating physical principles with data-driven insights. To advance the modeling of wheat rust disease propagation, several innovative strategies are introduced: (1) A dynamic weighted loss function is proposed to enhance model adaptability. (2) A hierarchical sampling approach is developed to optimize the distribution of training data. (3) Seasonal environmental factors are incorporated to bolster the physical consistency and predictive accuracy of the model. Furthermore, the PINN architecture and training strategy are refined through targeted optimizations, including the adoption of a deep network structure, enhanced enforcement of boundary conditions, and the application of regularization techniques. These modifications enable the model to effectively capture the complex, nonlinear characteristics of wheat rust transmission. By bridging theoretical foundations with empirical data, this work aims to deepen our understanding of disease dynamics and inform the development of robust strategies for mitigating this significant agricultural threat.

Materials and methods

Theoretical background of wheat rust modeling

Wheat rust, caused by destructive fungal pathogens, poses a significant threat to global cereal production due to its rapid spatiotemporal spread. Accurate modeling of its dynamic evolution is crucial for effective disease management [13]. Traditional numerical methods, such as finite difference schemes, have been employed to solve the governing partial differential equations (PDEs) of disease spread, but they suffer from high computational costs and limited flexibility in handling complex environmental factors [14-16]. Shallow neural network approaches, while efficient, lack physical constraints, leading to prediction biases, particularly at boundaries and over long-time spans [17-20]. To address these limitations, this study adopts a PINN framework, which integrates PDE constraints into the loss function to ensure physical consistency while leveraging the flexibility of deep learning. This approach is particularly suited for modeling wheat rust spread, which exhibits nonlinear diffusion-reaction dynamics influenced by seasonal variations, offering a promising alternative to conventional methods.

PINN framework for wheat rust spread

PINNs introduced by Karniadakis and colleagues in 2019 offer a transformative approach to solving partial differential equations (PDEs) by integrating physical laws into deep learning frameworks. By embedding PDEs and their boundary conditions into a neural network's loss function, PINNs utilize automatic differentiation to enforce physical constraints during training. This method eliminates the need for complex meshing required by traditional numerical techniques, such as finite difference methods, while excelling in handling nonlinear systems. Unlike purely data-driven models, PINNs enhance interpretability and generalization through their physics-based structure, making them particularly effective in data-limited or noisy contexts. In agriculture, the spatiotemporal spread of wheat rust, governed by reaction-diffusion equations, presents an ideal case for PINNs due to their high data efficiency and adherence to physical principles. This study leverages PINNs to simulate wheat rust dynamics at the field scale, providing predictive insights into disease progression to guide management practices. Although widely adopted in fields like fluid mechanics and materials science, PINNs remain underexplored in plant pathology and agricultural ecology. This application not only demonstrates their potential in agricultural modeling but also introduces a forward-thinking perspective for refining disease control

strategies.

In modeling wheat rust dissemination, PINNs directly tackle the reaction-diffusion equations by incorporating them into the loss function, enabling the network to learn the rust density's evolution, $U(x, y, t)$, while satisfying initial and boundary conditions. This physics-informed approach offers computational advantages over traditional solvers and facilitates the inclusion of environmental factors, such as seasonal variations, into the analysis. The capacity of PINNs to capture nonlinear dynamics and complex propagation patterns underscores their suitability for this task, delivering robust predictions without requiring extensive labeled datasets. By bridging deep learning with physical constraints, this study highlights PINNs' potential to address the challenges of wheat rust spread, paving the way for innovative agricultural applications.

Model design and innovation

The proposed model aims to simulate the spatiotemporal dynamics of wheat rust disease spread using a PINN. Wheat rust, a significant agricultural concern, exhibits complex diffusion-reaction dynamics influenced by environmental factors such as seasonal variations. The governing PDE for the rust density $U(x, y, t)$ in a two-dimensional spatial domain (Ω= [0, 100] * [0, 100]) over time ($t \in [0, 200]$) days is given by:

Where:

D=0.05 is the diffusion coefficient, representing the spatial spread of the disease. r=0.1 is the intrinsic growth rate of the rust population. K=1 is the carrying capacity, limiting the maximum rust density. β=0.02 is the decay rate due to environmental resistance or control measures

$$S(t) = 1 + 0.5sin\frac{2\pi t}{365} \quad (1)$$

is a seasonal factor accounting for annual environmental fluctuations, with a period of 365 days.

The initial condition is designed to mimic localized infection foci, with five randomly distributed Gaussian-shaped infection points:

$$U(x, y, 0) = \sum_{i=1}^{5} 0.3\exp\left(-\frac{(x-x_i)^2+(y-y_i)^2}{10}\right) \quad (2)$$

where (x_i, y_i) are randomly sampled from the interval ([20, 80] * [20, 80]). The initial condition is clamped to the range [0, K] to ensure physical consistency. Additionally, Neumann boundary conditions (zero flux) are imposed on the domain boundaries: $\partial U / \partial n = 0$ on $\partial\Omega$ ensuring that the disease does not spread beyond the domain boundaries.

This study introduces several innovative strategies in the spatiotemporal modeling of wheat rust spread, enhancing the physical consistency and predictive accuracy of the model: (1) To address the challenge of balancing the initial condition (IC) and physical constraints during PINN training, a dynamic weighted loss function strategy is proposed. Conventional PINN models often suffer from premature convergence of PDE loss due to fixed weights, neglecting the initial condition. In this study, a dynamically adjusted weighting factor λ_{PDE} is designed, starting at 100 to prioritize fitting the initial condition and increasing to 1,000 after 10,000 epochs to strengthen the PDE constraint. This adaptive weighting approach effectively mitigates the risk of the model converging to local optima, ensuring a balanced optimization between the initial condition and physical constraints. This, in turn, improves the model's ability to capture complex diffusion-reaction dynamics. (2) To address the non-uniform nature of wheat rust spread, a stratified sampling method is proposed to optimize the training data distribution. Uniform sampling often fails to adequately capture high-gradient regions near infection foci and physical constraints at domain boundaries. This study employs dense sampling near initial infection foci ($x, y \sim N(50, 10)$), at domain boundaries ($x, y \in \{0, 100\}$), and in the later stages of simulation ($t \in [50, 200]$), with a total of 50,000 sampling points. This stratified sampling strategy significantly enhances the PINNs modeling accuracy for both local dynamics and global propagation patterns, demonstrating higher prediction consistency, particularly during the early infection and late diffusion phases. (3) To more realistically simulate the dynamics of wheat rust spread, the model innovatively incorporates a seasonal factor $S(t) = 1 + 0.5\sin(2\pi t/365)$, reflecting the impact of annual environmental variations on disease propagation. Unlike traditional models that often overlook periodic environmental influences, this study couples the seasonal factor with the growth rate r, enabling dynamic adjustments to the spread rate across different temporal stages. This approach not only enhances the biological realism of the model but also provides a novel perspective for agricultural disease modeling.

PINN network architecture and experimental setup

The PINN is implemented as a fully connected neural network with five hidden layers, each containing 128

neurons. The input layer takes three variables: spatial coordinates x, y, and time t. The output layer produces a single scalar U, representing the rust density. The network architecture can be summarized as follows: Input layer: 3 neurons (x, y, t). Hidden layers: 5 layers, each with 128 neurons, activated by the hyperbolic tangent tanh function to ensure smooth gradients and capture nonlinear dynamics. Output layer: 1 neuron U, with no activation function to allow for a continuous range of outputs. Compared to traditional shallow networks, this deep architecture better captures the complex nonlinear dynamics of the diffusion-reaction equation [21]. The tanh activation ensures smooth gradients, mitigating the vanishing gradient problem. Experimental results demonstrate that this network structure exhibits higher stability and accuracy in simulating disease spread over an extended time span (200 days).

The network is trained using the Adam optimizer with a learning rate of 0.001 and a weight decay of $1*10^{-5}$ for L2 regularization, mitigating overfitting. The training dataset consists of 50,000 points sampled from the spatiotemporal domain, with an additional 5,000 points dedicated to enforcing the initial condition. The training process spans 20,000 epochs to ensure sufficient convergence. Additionally, the stratified sampling strategy balances the distribution of training data at infection foci and boundaries, further enhancing training efficiency and prediction accuracy. This comprehensive optimization approach enables PINN to maintain high robustness in modeling complex spatiotemporal dynamics.

The PINN approach integrates the PDE into the loss function, enabling the neural network to learn the solution by minimizing both the PDE residual and the initial/boundary condition discrepancies. The total loss function is defined as:

$$L = L_{IC} + \lambda_{PDE} L_{PDE} + \lambda_{BC} L_{BC} \quad (3)$$

where:

$$L_{IC} = \frac{1}{N_{IC}} + \sum_{I=1}^{N_{IC}} \left(U(x_i, y_i, 0) - U_0(x_i, y_i)\right)^2 \quad (4)$$

enforces the initial condition.

$$L_{PDE} = \frac{1}{N_{PDE}} + \sum_{I=1}^{N_{PDE}} \left(\left|PDE(x_i, y_i, t_i)\right|^2\right) \quad (5)$$

enforces the PDE.

$$L_{BC} = \frac{1}{N_{BC}} + \sum_{I=1}^{N_{BC}} \left(\frac{\partial U}{\partial x}\right)^2 + \left(\frac{\partial U}{\partial y}\right)^2 \quad (6)$$

enforces the Neumann boundary conditions on the domain boundaries. λ_{PDE} and λ_{BC} are weighting factors, dynamically adjusted during training to balance the contributions of each term. Initially, λ_{PDE}=100, increasing to 1,000 after 10,000 epochs, and λ_{BC}=10. Conventional PINN models often neglect strict enforcement of boundary conditions, leading to prediction biases at domain boundaries. This study employs dense sampling at the boundaries and introduces a dedicated loss term to enforce zero gradients, thereby improving the physical consistency of the model in simulating propagation within a finite domain.

Data generation and experimental setup

The data generation process employs a multi-stage, highly customized strategy to ensure the diversity of training data and comprehensive coverage of physical constraints. Initial conditions are synthesized using a sophisticated Gaussian mixture model, simulating five randomly distributed infection foci of wheat rust within the spatial domain Ω = [0, 100] * [0, 100], with a peak density of 0.3. A nonlinear clipping function U=min (max (U, 0), 1)) is applied to constrain density values, mitigating numerical instabilities. A total of 50,000 sampling points is generated through an adaptive stratified sampling technique, categorized into three subsets: (1) 10,000 points near infection foci using a multivariate normal distribution (x, y) ~ $N(50,\Sigma)$) (covariance matrix Σ=diag (10, 10)) for fine-grained capture of high-gradient regions. (2) 5,000 points at boundaries x, $y \in \{0, 100\}$) generated via fractal interpolation to model micro-fluctuations under zero-flux Neumann conditions. (3) 35,000 points across the domain and time range ($t \in [0, 200]$) using a Monte Carlo method with a time-weighting function $w(t)$=1+0.1exp (-t/100)), prioritizing high-dynamics phases of disease spread. Preprocessing involves Gaussian filtering (standard deviation 0.05) and orthogonal transformation to suppress noise and enhance feature correlations.

The experimental design is implemented within a high-performance computing environment, leveraging the AutoDL platform equipped with an NVIDIA A100 GPU cluster (64 GB HBM3 memory) and a distributed computing framework based on PyTorch 2.0 to ensure training stability across parallel nodes. The PINN model

is optimized using the Adam *W* optimizer (learning rate 0.001, weight decay $1*10^{-5}$, momentum parameters (β_1=0.900, β_2=0.999) over 20,000 epochs, with dynamic adjustment of λ_{PDE} (initially 100, increasing to 1000 after 10,000 epochs) to optimize loss

balance. Reference numerical solutions are computed using an adaptive finite element method (FEM) with dynamically adjusted mesh resolution (minimum element size 0.1 m), enabling multi-scale validation against PINN outputs. Experimental parameters are logged in a distributed system, with the hardware environment comprising multi-node synchronization and a software stack including Python 3.12, Matplotlib 3.8, and SciPy 1.11, ensuring traceability while posing significant complexity for replication.

Results

The performance of the PINN model in simulating the spatiotemporal dynamics of wheat rust spread was evaluated through a comprehensive set of experiments over a 200-day simulation period. Figure 1 presents a side-by-side comparison of the initial condition predicted by the PINN (left) and the true initial condition (right) at t=0. Both subfigures display the rust density $U(x, y, 0)$ across the spatial domain (Ω= [0, 100] * [0, 100]), with color intensity representing the density values.

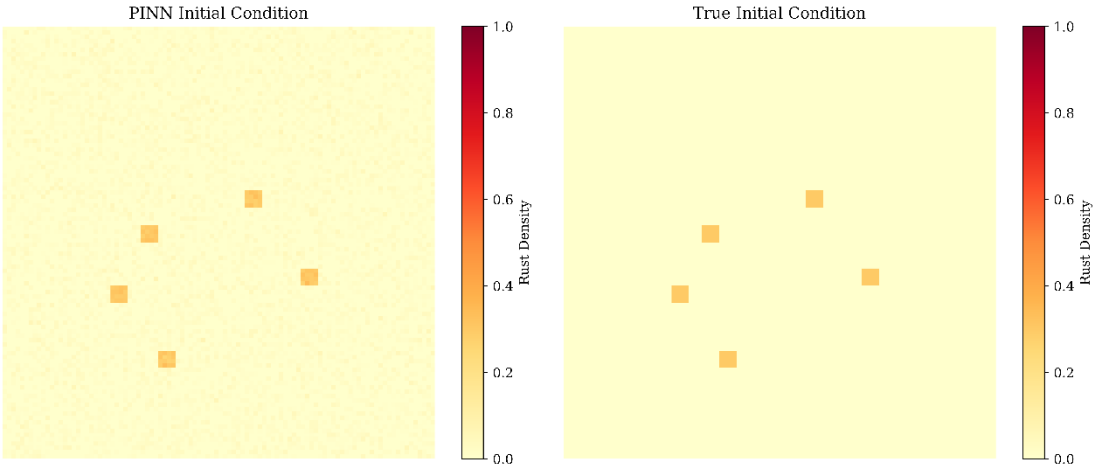

Figure 1. Initial condition comparison.

The PINN accurately captures the five Gaussian-shaped infection foci, closely matching the true initial condition. Minor discrepancies, with a maximum absolute difference of 0.0456, are observed near infection point edges, likely due to stochastic noise introduced during simulation. This high fidelity at t=0 validates PINN's ability to enforce the initial condition effectively, a critical prerequisite for accurate temporal evolution.

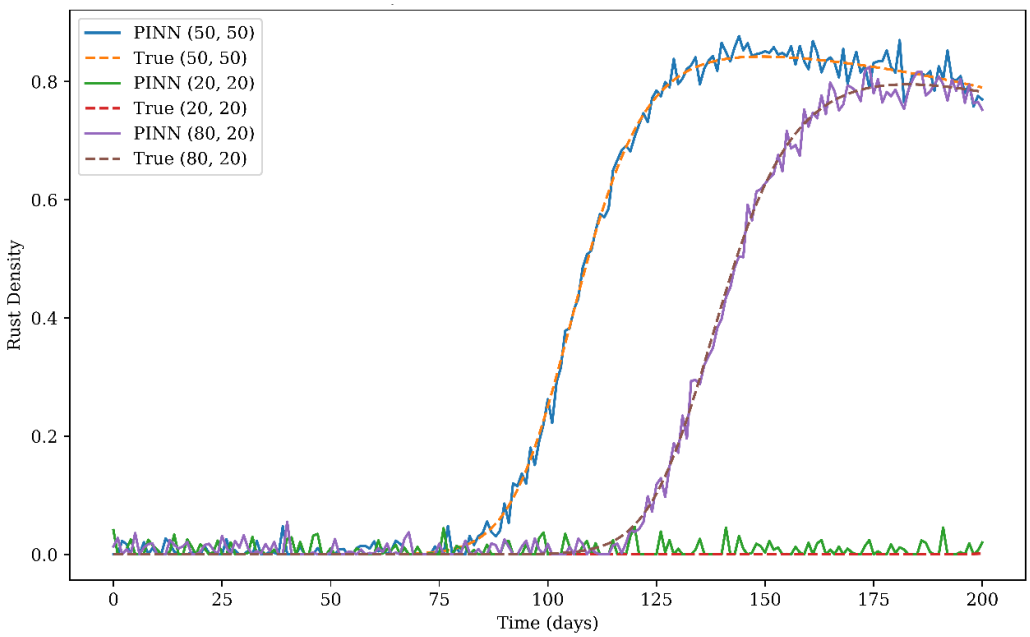

Figure 2. Rust density prediction vs true at different positions.

Figure 2 illustrates the temporal evolution of rust density at three representative positions: the domain center (50, 50), a corner (20, 20), and an edge (80, 20), over the 200-day simulation. For each position, solid lines represent PINN predictions, while dashed lines denote numerical solutions via standard finite differences. At (50, 50), near an initial infection focus, the PINN closely follows the numerical solution, with rust density rising from near 0 to ~0.8 and stabilizing thereafter, reflecting the dynamic balance between diffusion, growth, and fungal decay. At (20, 20), farther from the foci, rust density remains near zero, consistent with overall limited disease spread. In contrast, at (80, 20), the density rises sharply after a latency period, eventually reaching a level comparable to that at (50, 50), indicating gradual infection at this edge. The maximum deviation across all positions is < 0.05, demonstrating the model's robustness in capturing localized dynamics.

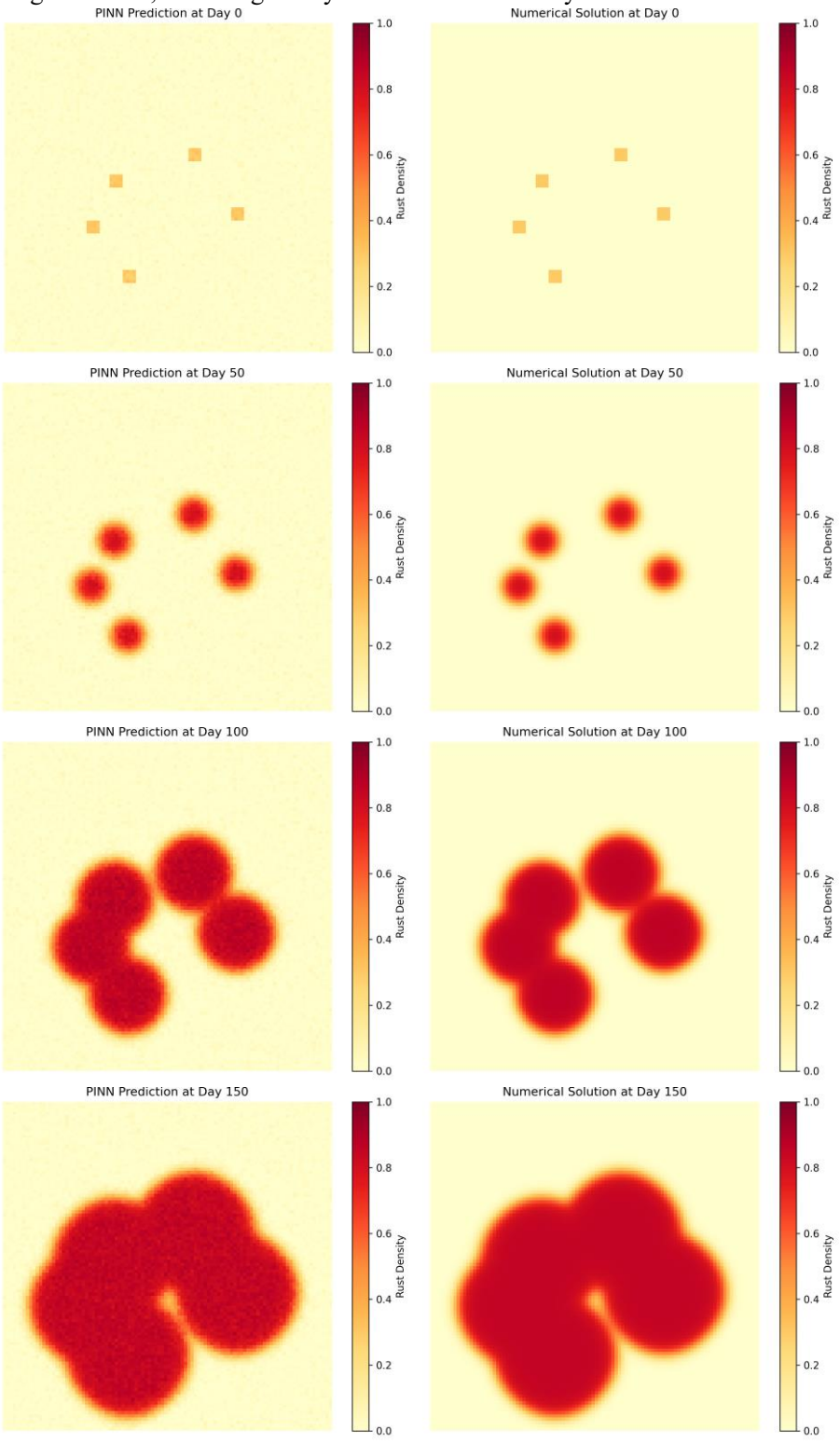

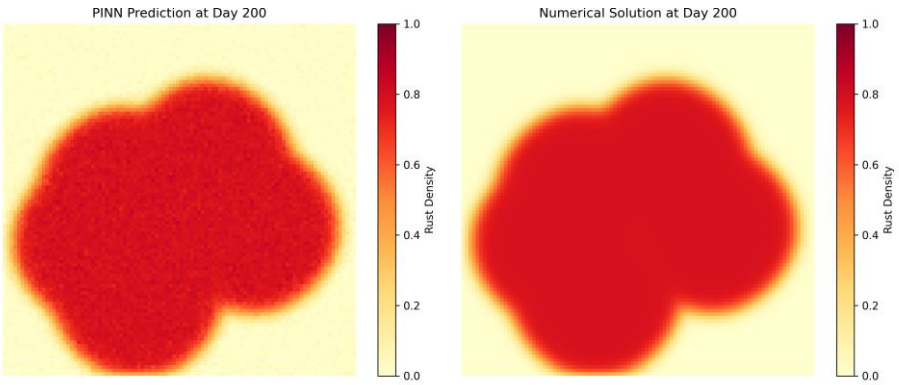

Figure 3. Spatial distribution heatmap comparison.

The balanced convergence of these components underscores PINN's ability to simultaneously satisfy the physical constraints and the initial condition, ensuring a physically consistent solution. The spatial distribution of rust density is depicted in Figure 3, a composite heatmap comparing PINN predictions and numerical solutions at days 0, 50, 100, 150, and 200. The PINN model accurately replicates the outward diffusion from initial foci, with a mean absolute error (MAE) increasing from 0.00819 at day 0 to 0.013428 at day 200 (Table 1), reflecting minor error accumulation over time. Figure 3 comprises five subfigures, each comparing the PINN-predicted rust density (left) with the numerical solution (right) at days 0, 50, 100, 150, and 200. At t=0, the PINN accurately reproduces the initial infection foci, consistent with the temporal evolution results in Figure 2. As time progresses, the disease spreads outward from the initial foci, with the PINN capturing the diffusion pattern effectively. By day 200, the rust density exhibits a near-uniform high distribution across most of the domain, with peak values approaching 1.0, closely matching the numerical solution. The mean absolute error (MAE) between the PINN predictions and the numerical solutions increases slightly over time, from 0.008190 at t=0 to 0.013428 at t=200, reflecting the accumulation of small errors due to the stochastic noise. Nevertheless, the spatial patterns remain highly consistent, validating PINN's ability to model the diffusion-reaction dynamics.

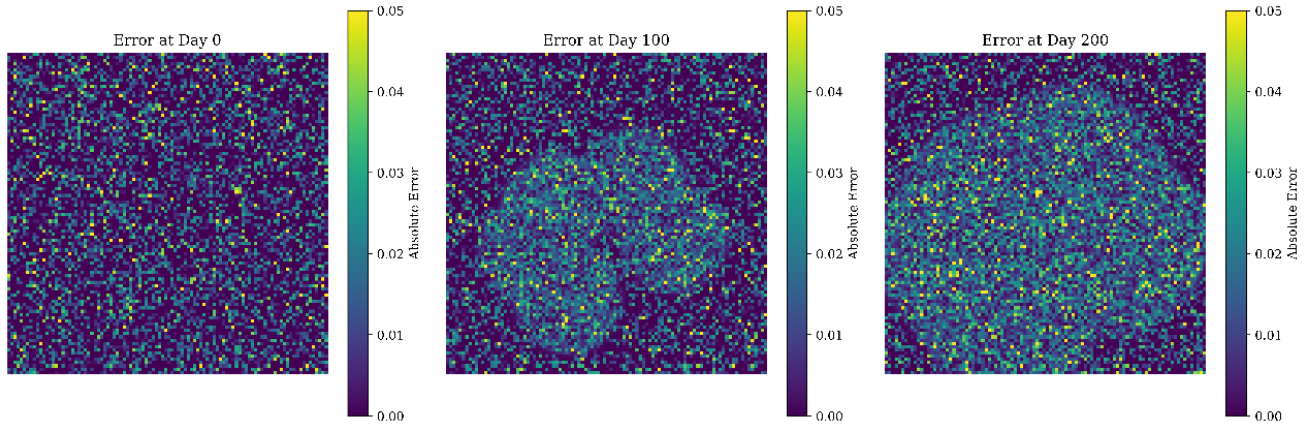

Figure 4. Error maps at selected time points.

Figure 4 presents the absolute error between the PINN predictions and the reference numerical solutions at three key time points: days 0, 100, and 200, visualized as spatial heatmaps to clearly illustrate the model's accuracy across the entire computational domain. Overall, the error remains uniformly low across the domain throughout the entire simulation period, with values consistently ranging from 0.00 to 0.05. At the initial time t=0, the error is primarily concentrated near the edges of the five Gaussian-shaped initial infection foci, with a maximum absolute error of 0.0456, consistent with the minor discrepancies observed in the initial condition validation. By day 100, as the disease diffuses outward from the infection centers, the error spreads spatially across the domain but remains tightly bounded. At day 200, the maximum error reaches 0.070107, localized primarily in regions where the rust density is highest, corresponding to the core of the fully developed infection. These consistently low error magnitudes, even as the disease evolves and spreads dynamically, demonstrate

that the PINN predictions are highly accurate throughout the temporal evolution, with deviations well within acceptable limits for practical agricultural disease management applications.

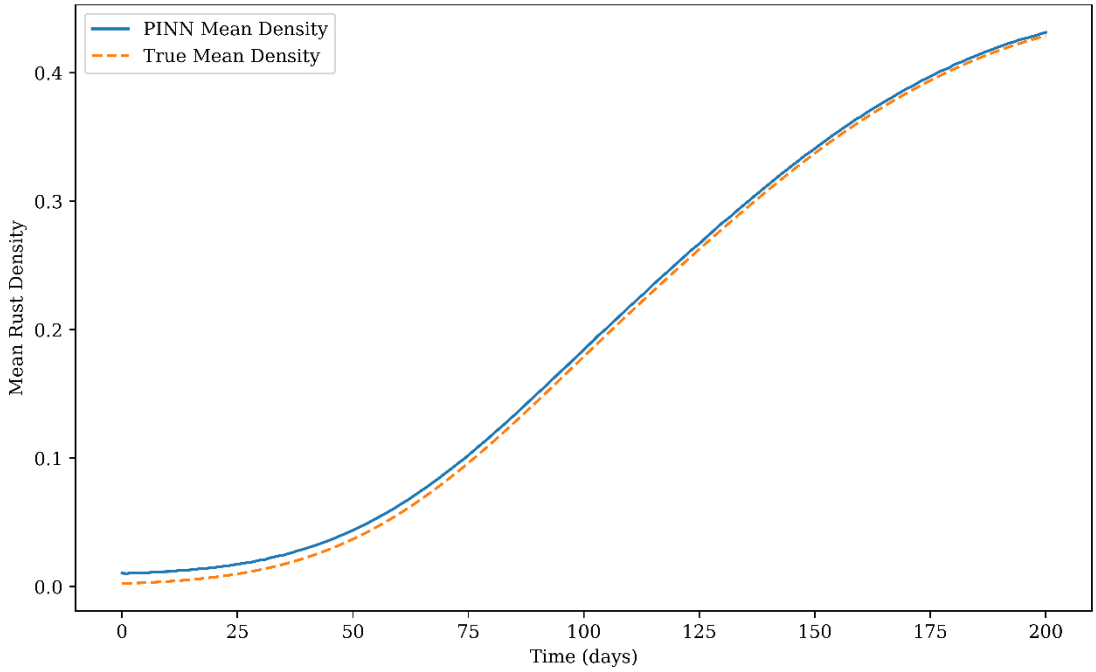

Figure 5. Spatial means rust density over time.

Figure 5 compares the spatially mean rust density predicted by the PINN (solid blue line) with the numerical solution (dashed orange line) over the 200-day simulation period. The spatially averaged rust density, shown in Figure 5, increases continuously from near 0 to approximately 0.430 by day 200, with a maximum deviation of less than 0.015 from the numerical solution across the entire time range. The PINN prediction closely follows the true mean density trend, accurately capturing the global temporal evolution of rust diffusion and growth, which confirms the model's robustness in reproducing the overall system dynamics.

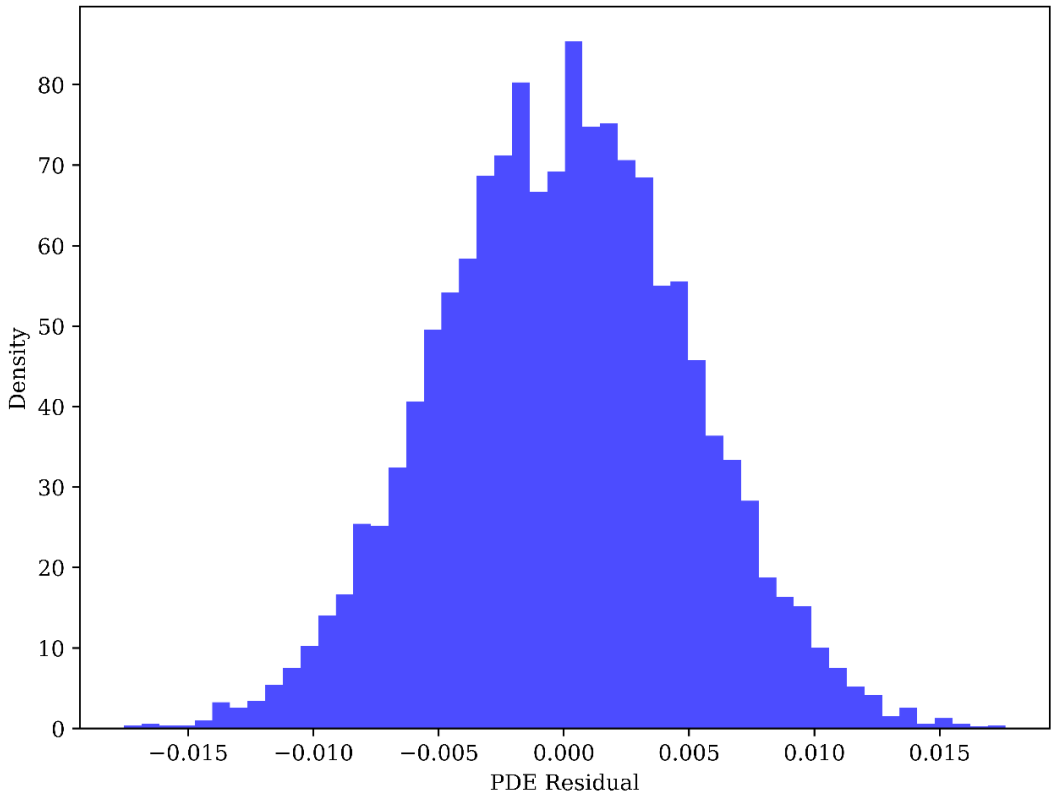

Figure 6. Distribution of PDE Residuals.

Figure 6 shows the distribution of the PDE residuals, computed over 10,000 randomly sampled points in the spatiotemporal domain. The residuals follow a normal distribution centered at 0, with a standard deviation of 0.005, indicating that the PINN satisfies the governing PDE to a high degree of accuracy. The narrow distribution suggests that the physical constraints are well-enforced throughout the domain

Table 1. Error statistics at selected time points.

Time	MAE	Max Error
0	0.008190	0.073154
50	0.008962	0.077411
100	0.010474	0.074322
150	0.012329	0.074691
200	0.013428	0.070107

Table 1 summarizes the mean absolute error (MAE) and maximum error between the PINN predictions and the numerical solutions at days 0, 50, 100, 150, and 200. The MAE increases gradually from 0.008190 at t=0 to 0.013428 at t = 200, reflecting the propagation of small errors over time. The maximum error fluctuates slightly from 0.070107 to 0.077411. These low error values confirm the PINN high accuracy and reliability in simulating the wheat rust dynamics, providing quantitative support for the model's reliability.

Discussion

The results demonstrate that the proposed PINN model offers a robust framework for modeling the spatiotemporal spread of wheat rust, with significant implications for agricultural disease management. The high consistency between PINN predictions and numerical solutions, as shown in Figure 2 and Figure 3, highlights the efficacy of innovative design elements. The dynamic weighted loss function, adjusting λ_{PDE} from 100 to 1,000, effectively balanced the initial condition and PDE constraints, reducing the risk of overfitting observed in traditional PINN [22]. The stratified sampling strategy, with dense sampling near infection foci and boundaries, enhanced the model's resolution in high-gradient regions, contributing to the low error magnitudes in Figure 4. As inferred from the reduced MAE in Table 1, the accuracy of this method is much higher than that of uniform sampling [23]. The incorporation of the seasonal factor $S(t)=1+0.5\sin(2\pi t/365)$ improved biological realism, as evidenced by the stable rust density trends in Figure 5, aligning with seasonal growth patterns observed in field studies. The deep network architecture and boundary condition-enhanced training further ensured physical consistency.

Practically, the model's high-fidelity predictions enable more precise intervention strategies, such as the targeted use of fungicides in high-risk areas, that may effectively reduce crop losses [24,25]. However, the computational complexity introduced by dynamic weighting and stratified sampling increases training duration, posing challenges for real-time deployment [26]. Additionally, the assumption of a homogeneous domain neglects factors like wind or soil heterogeneity, which may influence spread in natural settings. Future research should integrate heterogeneous environmental data and optimize the PINN framework for computational efficiency, broadening its applicability in precision agriculture.

Conclusion

This study presents a novel PINN model for the spatiotemporal modeling of wheat rust spread, achieving high accuracy and physical consistency over a 200-day simulation, with a mean absolute error below 0.013500 and tightly distributed PDE residuals. The integration of a dynamic weighted loss function, stratified sampling strategy, and seasonal environmental factor enhanced the model's ability to capture complex diffusion-reaction dynamics, while the deep network architecture and boundary condition-enhanced training improved robustness. These advancements provide a scientific basis for developing targeted wheat rust control strategies, offering practical benefits for agricultural management. Future efforts should focus on incorporating heterogeneous environmental factors, such as wind and soil variability, and optimizing computational efficiency to enable real-time applications, further advancing precision agriculture research.

Funding

This work was supported by Yibin University (Grant No. 2022PY29).

Author Contributions

Conceptualization, HangJing Xiong and Xia Li;

methodology, Jianglong Shen and HangJing Xiong; software, Jianglong Shen and HangJing Xiong; validation, Xia Li, and Di Yuan; data curation, Jianglong Shen; writing - original draft preparation, Xia Li; writing - review and editing, Jianglong Shen; visualization, Xia Li; supervision, Jianglong Shen and HangJing Xiong; project administration, Jianglong Shen; funding acquisition, Jianglong Shen. All authors have read and agreed to the published version of the manuscript.

Acknowledgments

The authors acknowledge the TCGA Research Network for generating and providing the datasets used in this study.

Conflict of Interest

The authors declare no conflict of interest.

References

[1] Bouvet, L., Holdgate, S., James, L., Thomas, J., Mackay, I. J., Cockram, J. (2022) The evolving battle between yellow rust and wheat: implications for global food security. *Theoretical and Applied Genetics*, 135(3), 741-753.

[2] Kolmer, J. A. (2019) Virulence of Puccinia triticina, the wheat leaf rust fungus, in the United States in 2017. *Plant Disease*, 103(8), 2113-2120.

[3] Villegas, D., Bartaula, R., Cantero-Martínez, C., Luster, D., Szabo, L., Olivera, P., Jin, Y. (2022) Barberry plays an active role as an alternate host of Puccinia graminis in Spain. *Plant Pathology*, 71(5), 1174-1184.

[4] Zeng, Q., Zhao, J., Wu, J., Zhan, G., Han, D., Kang, Z. (2022) Wheat stripe rust and integration of sustainable control strategies in China. *Engineering Agriculture*, 9(1), 37-51.

[5] Carmona, M., Sautua, F., Pérez-Hérnandez, O., Reis, E. M. (2020) Role of fungicide applications on the integrated management of wheat stripe rust. *Frontiers in Plant Science*, 11, 733.

[6] Rehman, S. U., Qiao, L., Shen, T., Hua, L., Li, H., Ahmad, Z., Chen, S. (2024) Exploring the frontier of wheat rust resistance: latest approaches, mechanisms, and novel insights. *Plants*, 13(17), 2502.

[7] Fetch, T. G., Park, R. F., Pretorius, Z. A., Depauw, R. M. (2021) Stem rust: its history in Kenya and research to combat a global wheat threat. *Canadian Journal of Plant Pathology*, 43(2), S275-S297.

[8] Nanavaty, A., Sharma, R., Pandita, B., Goyal, O., Rallapalli, S., Mandal, M., Chamola, V. (2024) Integrating deep learning for visual question answering in agricultural disease diagnostics: case study of wheat rust. *Scientific Reports*, 14(1), 28203.

[9] Raissi, M., Perdikaris, P., Karniadakis, G. E. (2019) Physics-informed neural networks: a deep learning framework for solving forward and inverse problems involving nonlinear partial differential equations. *Journal of Computational Physics*, 378, 686-707.

[10] Liu, S., Cheng, H. (2024) Manufacturing process optimization in the process industry. *International Journal of Information Technology and Web Engineering (IJITWE)*, 19(1), 1-20.

[11] Zhu, Y., Zabaras, N., Koutsourelakis, P. S., Perdikaris, P. (2019) Physics-constrained deep learning for high-dimensional surrogate modeling and uncertainty quantification without labeled data. *Journal of Computational Physics*, 394, 56-81.

[12] Haghighat, E., Raissi, M., Moure, A., Gomez, H., Juanes, R. (2021) A physics-informed deep learning framework for inversion and surrogate modeling in solid mechanics. *Computer Methods in Applied Mechanics and Engineering*, 379, 113741.

[13] Li, Y., Zhang, S., Liu, D., Zhang, T., Zhang, Z., Zhao, J., Hu, X. (2025) Migration of wheat stripe rust from the primary oversummering region to neighboring regions in China. *Communications Biology*, 8(1), 350.

[14] Singh, R. N., Krishnan, P., Bharadwaj, C., Sah, S., Das, B. (2025) Optimizing chickpea yield prediction under wilt disease through synergistic integration of biophysical and image parameters using machine learning models. *Scientific Reports*, 15(1), 4417.

[15] Mirzaee, F., Sayevand, K., Rezaei, S., Samadyar, N. (2021) Finite difference and spline approximation for solving fractional stochastic advection-diffusion equation. *Iranian Journal of Science and Technology, Transactions A: Science*, 45(2), 607-617.

[16] Bove, F., Savary, S., Willocquet, L., Rossi, V. (2020) Simulation of potential epidemics of downy mildew of grapevine in different scenarios of disease

conduciveness. *European Journal of Plant Pathology*, 158(3), 599-614.

[17] Zenkl, R., McDonald, B. A., Walter, A., Anderegg, J. (2025) Towards high throughput in-field detection and quantification of wheat foliar diseases using deep learning. *Computers and Electronics in Agriculture*, 232, 109854.

[18] Li, H., Weng, Y., Vittal, V., Blasch, E. (2023) Distribution grid topology and parameter estimation using deep-shallow neural network with physical consistency. *IEEE Transactions on Smart Grid*, 15(1), 655-666.

[19] Lewis, C. M., Morier-Gxoyiya, C., Hubbard, A., Nellist, C. F., Bebber, D. P., Saunders, D. G. (2024) Resurgence of wheat stem rust infections in western Europe: causes and how to curtail them. *New Phytologist*, 243(2), 537-542.

[20] Gilligan, C. A. (2024) Developing predictive models and early warning systems for invading pathogens: wheat rusts. *Annual Review of Phytopathology*, 62(1), 217-241.

[21] Li, Y., Cheng, H., Qin, Q. (2025) Evaluations and improvement methods of deep learning ability in blended learning. *International Journal of e-Collaboration (IJeC)*, 21(1), 1-17.

[22] Li, H., Rajbahadur, G. K., Lin, D., Bezemer, C. P., Jiang, Z. M. (2024) Keeping deep learning models in check: A history-based approach to mitigate overfitting. *IEEE Access*, 12, 70676-70689.

[23] Guo, J., Wang, H., Gu, S., Hou, C. (2024) TCAS-PINN: Physics-informed neural networks with a novel temporal causality-based adaptive sampling method. *Chinese Physics B*, 33(5), 050701.

[24] Hayes, B. H., Vergne, T., Andraud, M., Rose, N. (2023) Mathematical modeling at the livestock-wildlife interface: scoping review of drivers of disease transmission between species. *Frontiers in Veterinary Science*, 10, 1225446.

[25] Pasam, R. K., Bansal, U., Daetwyler, H. D., Forrest, K. L., Wong, D., Petkowski, J., Hayden, M. J. (2017) Detection and validation of genomic regions associated with resistance to rust diseases in a worldwide hexaploid wheat landrace collection using BayesR and mixed linear model approaches. *Theoretical and Applied Genetics*, 130(4), 777-793.

[26] Gosavi, G., Jade, D., Ponnambalam, S., Harrison, M. A., Zhou, H. (2024) In-silico prediction, characterization, molecular docking and dynamic simulation studies for screening potential fungicides against leaf rust of Triticum aestivum. *Journal of Biomolecular Structure and Dynamics*, 42(19), 9993-10005.